Nanoscale

PAPER

View Article Online
View Journal | View Issue

Cite this: *Nanoscale*, 2024, **16**, 5294

Tip-enhanced Raman spectroscopy reveals the structural rearrangements of tau protein aggregates at the growth phase†

Kamila Sofińska, *[a] Sara Seweryn,[a,b] Katarzyna Skirlińska-Nosek,[a,b] Jakub Barbasz[c] and Ewelina Lipiec *[a]

Received 13th December 2023,
Accepted 1st February 2024

DOI: 10.1039/d3nr06365h

rsc.li/nanoscale

Tau protein aggregates inside neurons in the course of Alzheimer's disease (AD). Because of the enormous number of people suffering from AD, this disease has become one of the world's major health and social problems. The presence of tau lesions clearly correlates with cognitive impairments in AD patients, thus, tau is the target of potential treatments for AD, next to amyloid-β. The exact mechanism of tau aggregation has not been understood in detail so far; especially little is known about the structural rearrangements of tau aggregates at the growth phase. The research into tau conformation at each step of the aggregation pathway will contribute to the design of effective therapeutic approaches. To follow the secondary structure of individual tau aggregates at the growth phase, we applied tip-enhanced Raman spectroscopy (TERS). The nanospectroscopic approach enabled us to follow the structure of individual aggregates occurring in the subsequent phases of tau aggregation. We applied multivariate data analysis to extract the spectral differences for tau aggregates at different aggregation phases. Moreover, atomic force microscopy (AFM) allowed the tracking of the morphological alterations for species occurring with the progression of tau aggregation.

Neurodegenerative disorders with accompanying abnormal aggregation of proteins are some of the most serious health and social problems worldwide today.[1,2] Alzheimer's disease (AD) is the most common form of dementia, and it constitutes approximately 50–60% of total dementia cases.[1,3] In 2020, *ca.* 50 million people worldwide were suffering from dementia.[4] It is estimated that the number of individuals suffering from dementia will almost double every 20 years[5] because of an aging population and prolonged life expectancy.

The major histopathological hallmark of neurodegeneration involved in Alzheimer's disease is the presence of intraneuronal tau neurofibrillary tangles (NFTs) and extra-neuronal amyloid-β (Aβ) plaques in the neocortex.[6–9] The neuronal mechanism that links tau neurofibrillary tangles and amyloid-β plaques with neural system failure and cognitive decline in AD has not been fully understood.[7] However, amyloid-β and tau protein interact at synapses, causing simultaneous toxicity in the pathogenesis of AD.[6,10–12] Most of the Aβ targeting therapies have failed in clinical trials, thus, there is still a need for alternative strategies to fight against AD.[3,13–15] Because of a clear correlation of tau lesions with cognitive impairments, tau protein has also become a target for potential AD treatments.[3] In particular, small soluble oligomeric aggregates, found to be the most toxic species among various forms of tau aggregates present in the brain of AD patients, will be targets for future tau-oriented therapies against AD.[16,17]

Tau neurofibrillary tangles (NFTs) appear in neurons at a later stage of the disease.[3] This suggests that inhibiting tau aggregation at the early stages of the tau aggregation process could prevent neurodegenerative symptoms characteristic of the late stages of AD. Therefore, knowledge of the aggregation pathway and accompanying structural rearrangements occurring during tau neurofibrillary tangle (NFT) formation related to the disease etiology is of critical importance for the proper design of therapeutic strategies based on aggregation suppression. Despite the efforts of researchers representing numerous research disciplines, the molecular mechanisms mediating tau aggregation remain elusive.[18,19] There is still no cure for neurodegenerative disorders.[14]

The lack of selective techniques enabling the investigation of individual forms of protein during the aggregation process

[a]*Jagiellonian University, Faculty of Physics, Astronomy and Applied Computer Science, M. Smoluchowski Institute of Physics, Łojasiewicza 11, 30-348 Krakow, Poland. E-mail: kamila.sofinska@uj.edu.pl, ewelina.lipiec@uj.edu.pl*
[b]*Jagiellonian University, Doctoral School of Exact and Natural Sciences, Krakow, Poland*
[c]*Jerzy Haber Institute of Catalysis and Surface Chemistry Polish Academy of Sciences, Niezapominajek 8, 30-239 Krakow, Poland*

† Electronic supplementary information (ESI) available. See DOI: https://doi.org/10.1039/d3nr06365h

(oligomers, protofibrils and fibrils) has limited the possibility of exploring the knowledge regarding structural changes of aggregates occurring at the subsequent stages of this process, and thus, a complete understanding of the aggregation pathway. Conventional analytical techniques provide information averaged for a number of molecules at different stages of the aggregation process. Therefore, so far it has been possible to build only theoretical hypotheses regarding aggregation pathways without a detailed verification of structural transitions occurring in molecules during the course of this process over time.

Recent advances in molecular nanospectroscopy, specifically TERS (tip-enhanced Raman spectroscopy), showed that this technique was efficient for probing the structural rearrangements of proteins with the resolution of single protein aggregates.[20–23] TERS enables the acquisition of the Raman signal from individual molecules with nanometric spatial resolution.[21,23,24] Thus, it is possible to determine the local chemical structure and conformation of aggregating proteins. Structural characteristics of aggregating proteins and peptides have recently been studied with AFM-IR.[25–27] TERS and AFM-IR are complementary methods, both taking advantage of a combination of scanning probe microscopy (SPM) with molecular spectroscopy to deliver chemical information on a studied sample at the nanoscale. However, these two techniques exploit different physical phenomena to overcome the diffraction limit.[28] In TERS, the SPM tip acts as a nanoantenna which converts the propagating wave into the near field, and *vice versa*, the near field from the measured sample to the propagating wave. This antenna is the source of a well-defined electromagnetic field due to the collective movements of electrons (plasmons) in the nanostructure present at the SPM tip apex under irradiation with laser light. In AFM-IR, the laser illuminates the sample in close proximity to the AFM tip. The sample absorbs the electromagnetic radiation, which is followed by thermal expansion of the sample. Under the expansion, the sample located directly under the AFM tip pushes the cantilever, and the cantilever deflection, which is proportional to the IR absorption, is used.[28]

Both TERS and AFM-IR have a few minor pros and cons which make them slightly more suitable for other specific applications. For example, due to the high absorption of water, AFM-IR is challenging to implement for the measurement of aggregating proteins/peptides in water, while TERS has been already shown to deliver structural information on amyloid-β in a liquid environment.[20] On the other hand, infrared nanospectroscopy provides better contrast in the spectral range of amides, which delivers information about the secondary structures of proteins and peptides.[29] However, both methods provide complementary structural information at the nanoscale and can be interchangeably applied in investigations of aggregating amyloids.[20–22,25–27,30]

Here, we report on research into the chemical structure and conformation of tau protein aggregates at the growth phase of the aggregation process. While the structure of tau fibrils is dominated by the cross-β pattern, still little is known about the structural rearrangements occurring in the course of tau aggregation. Thus, we captured TER spectra for protofibrils and young fibrils at the early aggregation stage to reveal their structure and gain insights into the TER signature related to structural transitions resulting from the ongoing aggregation. We applied multivariate data analysis to treat the TERS data acquired from protofibrils and young fibrils to reveal discrepancies in the structure of tau aggregates in time.

To find a representative time point to explore the structure of tau protein aggregates at the early phase of the aggregation, we performed a comprehensive study of the time-dependent aggregation (0–336 h). We applied AFM imaging of tau species occurring in the studied time range of aggregation (Fig. 1A) and determined the length of the aggregates (Fig. 1B). Based on the AFM images, 24 and 72 h incubation times of tau protein (at 37 °C) were selected specifically to monitor the structure of tau aggregates *via* TERS before full fibrillation.

The AFM topography images of tau aggregates after 24 and 72 h together with cross-section profiles through oligomers (red profiles 1–3), protofibrils (green profiles 4–6) and fibrils (blue profiles 7–9) are presented in Fig. 1C. The extracted height cross-section profiles (Fig. 1C) clearly indicate the morphological diversity between tau aggregates at various aggregation stages: oligomers, protofibrils, and fibrils. For both 24 and 72 h of incubation, oligomeric intermediates characteristic of the initial aggregation stage display the lowest profiles (2.5–5 nm) with the smallest half-width. The height and the half-width of the profiles extracted for protofibrils (4–6) are exactly between those for oligomeric and fibrillar aggregates (*ca.* 5.2–6.2 nm). The profiles of fibrils are clearly the highest ones (*ca.* 6.2–8 nm) with the largest half-width.

To explore the TERS pattern of protofibrils and young fibrils, we acquired single point spectra at selected locations. In Fig. 2, TER spectra acquired from individual protofibrils and fibrils with the indicated locations of spectra acquisition marked on the corresponding AFM topography images are presented. TER spectra collected after 24 h of incubation display mainly bands characteristic of the initial aggregation phases. The prominent band in the spectral range between 1526 and 1514 cm^{-1} was attributed to anti-parallel β-sheets in amyloid-β aggregates in the protofibril form.[20] Depending on the location of spectra acquisition, the TER spectra of protofibrils incubated for 24 h also display the amide III bands indicating the presence of turns/random coil structures (1263–1248 cm^{-1}), anti-parallel β-sheets (1243 cm^{-1}), and parallel β-sheets (1228–1222 cm^{-1}).[20,22] Moreover, in the spectra of protofibrils, bands characteristic of phenylalanine can also be recognized, specifically the ring breathing mode at 1003 cm^{-1} and/or the ring deformation mode at *ca.* 1030 cm^{-1}.[31,32] In most spectra of protofibrils, TER bands in the amide I region are not well resolved. TER spectra acquired from young fibrils after 72 h of tau protein aggregation are rich in bands characteristic of proteins and fibrillar aggregates. Here, a well-resolved band at 1633–1628 cm^{-1} in the amide I region indicating the presence of parallel β-sheets was found in aggregated species at the advanced aggregation stage.[21] In the amide II region, intense

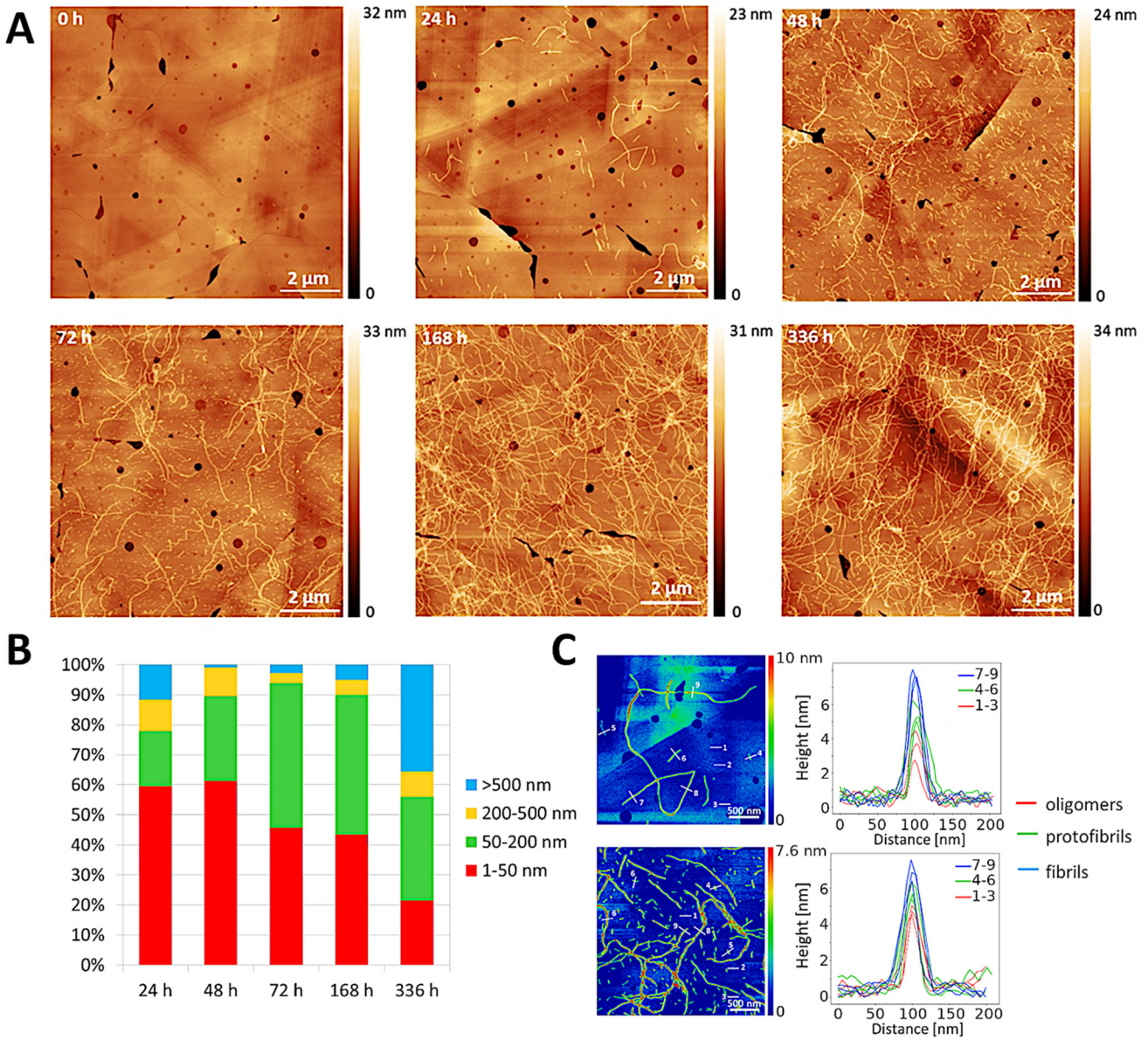

Fig. 1 Monitoring of morphological changes during the aggregation of tau protein: (A) AFM topography images of tau protein aggregating within 0–336 h, (B) ratios of tau aggregates displaying length of aggregates in the ranges: 1–50 nm, 50–200 nm, 200–500 nm, and above 500 nm, (C) AFM images of tau protein aggregating for 24 and 72 h together with cross-section profiles through oligomers, protofibrils, and fibrils.

bands in the spectral range of 1574–1552 cm^{-1} suggest the abundance of fibril core β-sheet/random coil structures in fibrillar aggregates.[20,33] The less intense band in this spectral region at 1539–1534 cm^{-1} may indicate the presence of α-helix secondary structure to a minor extent.[33,34]

All acquired spectra of young fibrils formed after 72 h of incubation display the intense band at 1490–1473 cm^{-1} attributed to N–H deformation of the heteroaromatic ring of histidine.[20,32,35] Additionally, a relatively weak band in the range of 1466–1433 cm^{-1} (CH, CH_2, and CH_3 deformation) is visible in the TER spectra.[35–37] The symmetric stretching of CO_2^- group is well defined at 1420–1403 cm^{-1}.[36,37] The C_α–H/N–H bending mode distinctive of β-sheets is pronounced in the range of 1397–1387 cm^{-1}.[20,37] In the amide III region, the band at 1340–1320 cm^{-1} of methylene deformation occurs with various intensities depending on the site of spectrum acquisition.[35,36] In this spectral range, bands typical of the secondary structure are also pronounced at 1267–1266 cm^{-1} (unordered structure),[22,33,36,37] 1241–1239 cm^{-1} (anti-parallel β-sheets),[20,22] and 1232–1214 cm^{-1} (parallel β-sheets).[20,22] In all TER spectra acquired from young fibrils, the band at 1182–1178 cm^{-1} is present. This spectral position is attributed to the N–H vibration of histidine or arginine,[31,35] and/or the C–H stretching of methionine,[31] and the C–H bending/C–O stretching vibrations of phenylalanine.[31] Finally, the band at *ca.* 1003 cm^{-1} is the most characteristic band for proteins

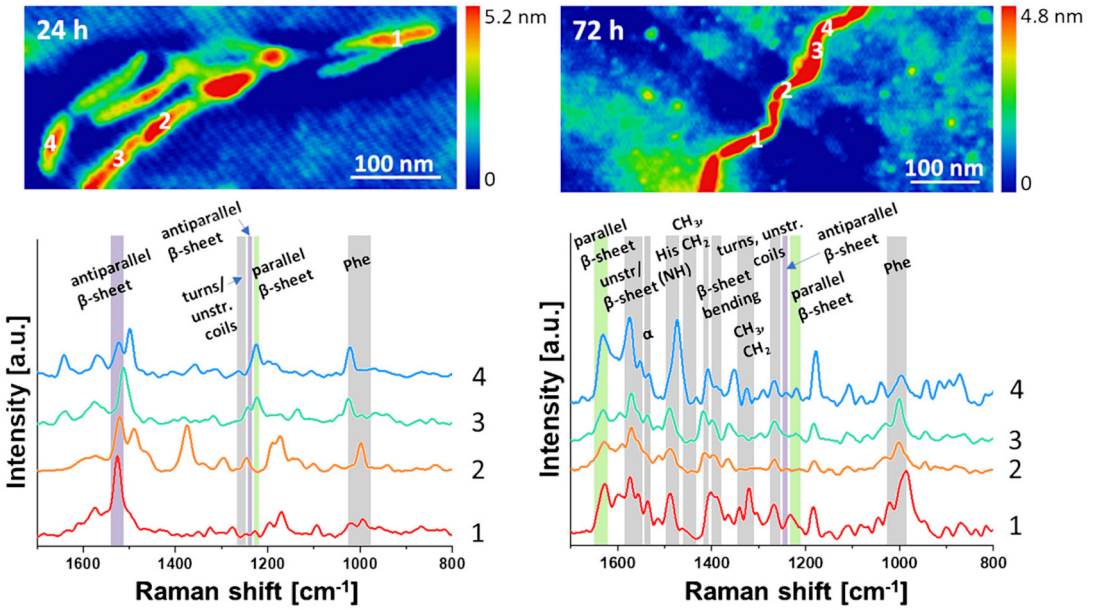

Fig. 2 Single point TER spectra with the corresponding AFM topographies containing indicated locations of the spectra acquisition. TER spectra were acquired from protofibrils after 24 h of incubation (left panel), and fibrils aggregating for 72 h (right panel). Parallel and anti-parallel β-sheets are indicated with green and purple bands, respectively.

attributed to a ring breathing mode of phenylalanine.[20,22,32] Numerous vibrational modes typical of β-sheets indicate the increase of the relative content of β-sheet secondary structure in comparison with protofibrillar aggregates.

We exploited multivariate data analysis to extract TERS band characteristics for tau protein aggregates at the growth phase of the aggregation process. Specifically, the principal component analysis (PCA) and hierarchical cluster analysis (HCA) were conducted on spectra collected from protofibrils after 24 h of incubation and young fibrils after 72 h of incubation in order to extract the most important information and spectral differences from the data. The results of PCA and HCA are presented in Fig. 3 and 4, respectively.

The PCA algorithm allows us to reduce the dimensionality of the collected spectral data and produces the scores and loading plots. The scores plot visually presents similarity or variability within the data based on the grouping along principal components (PCs). The loading plots of principal components present the spectral differences that determined the data separation. The results of PCA presented in Fig. 3 show that three main principal components were distinguished (PC1, PC2, and PC3), which together represent 77% of the total spectra variability. Therefore, the subgrouping along the first three PCs is statistically significant. However, the analyzed data show the strongest dependence on the PC1, which explains 33% of the total variance. The spectra acquired from protofibrils are located mainly along the positive values of PC1, while spectra of fibrils are grouped predominantly in the negative space of PC1. The loading plot of PC1 contains extremes characteristic of proteins. In particular, a prominent maximum is observed at 1521 cm^{-1} related to the anti-parallel β-sheet content in protofibrils.[20] Moreover, the maximum located at 1173 cm^{-1} was significant for the subgrouping of spectra acquired from tau aggregates after 24 h of incubation on the positive side of PC1. The bands present in the spectral region of 1200–1100 cm^{-1} are attributed to the vibrations of the side chains of amino acids. The location of the maximum at 1173 cm^{-1} may indicate the N–H vibration of histidine or arginine,[31,35] and/or the C–H stretching of methionine,[31] or the vibration of tyrosine.[38] The significant loading value at the negative side of the PC1 loading at 1627 cm^{-1} influenced the separation of spectra acquired from fibrils incubated for 72 h and the location of these data in the negative PC1 space. The position of this minimum suggests the increase of the parallel β-sheet content in young fibrils in comparison with protofibrils.[20] Thus, the structure of tau protein aggregates is ordering along the incubation into species composed of parallel β-sheets characteristic of mature fibrils. Additionally, the minimum at 1399 cm^{-1} of the PC1 loading attributed to β-sheet bending may indicate the increase in the relative content of β-sheets in fibrils formed after 72 h of incubation.[20]

The acquired TER spectra of protofibrils and young fibrils also display separation along PC2 (25% of the total variance). The spectra acquired from protofibrils are located predominantly in the negative PC2 space, which is driven by the minima of the PC2 loading located at 1496 cm^{-1} (histidine),[35,39] 1138 cm^{-1} (the NH^{3+} vibration of glutamine, asparagine, or isoleucine),[31,35] and 962 cm^{-1} (C_β wagging of histidine)[39] characteristic of amino acid residues. Moreover, the minimum at 1370 cm^{-1} of the PC2 loading indicates the C_α–H/N–H bending modes of β-sheets in protofibrils.[20,21,35,40] Spectra recorded from aggregates incubated for 72 h (young

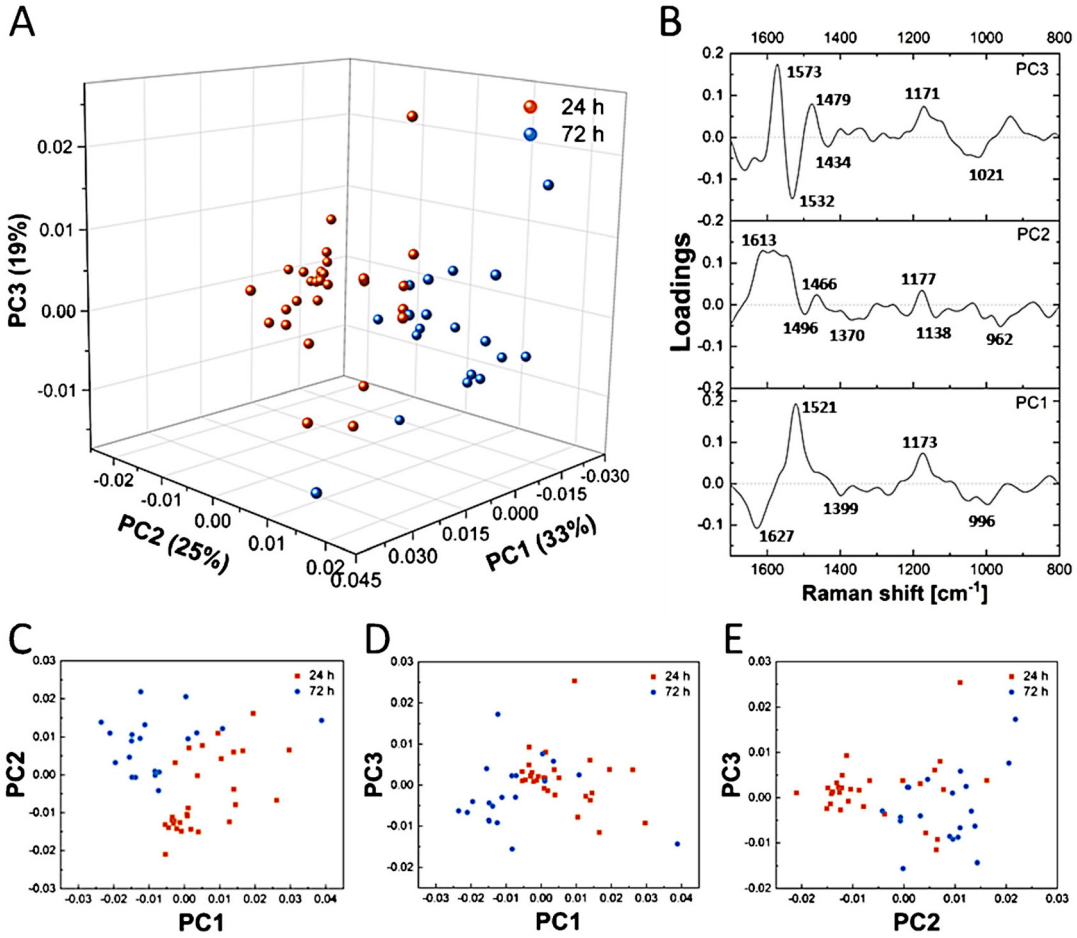

Fig. 3 The results of the principal component analysis (PCA) of spectra acquired from protofibrils after 24 h of incubation (orange), and fibrils after 72 h of incubation (blue): (A) the – 3D scores plot, (B) and loading plots for three first principal components (PCs); (C–E) 2D scores plots.

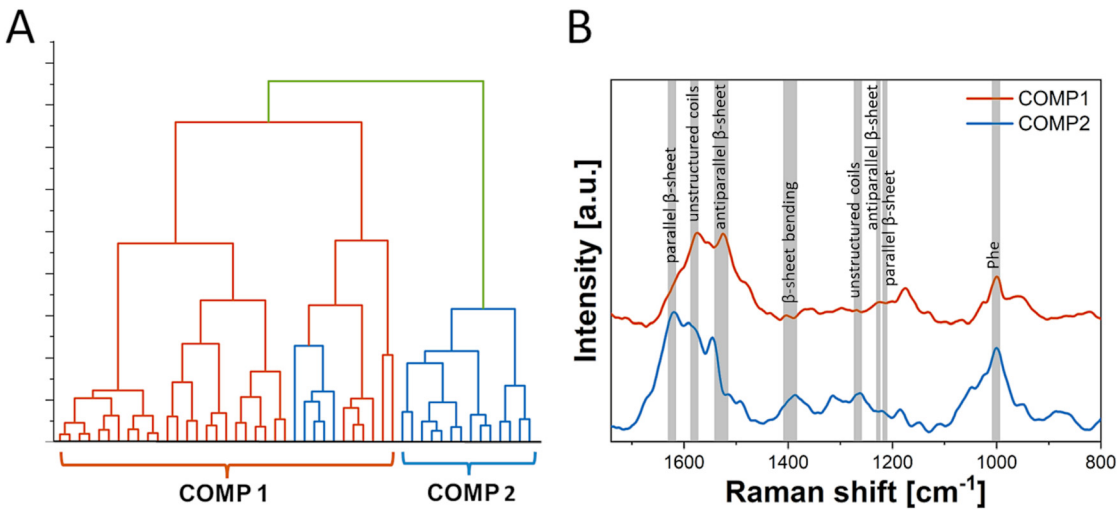

Fig. 4 The results of hierarchical cluster analysis (HCA) of spectra acquired from protofibrils after 24 h of incubation, and fibrils after 72 h of incubation: (A) dendrogram presenting the clustering and (B) mean spectra for each cluster.

fibrils) are located mostly on the positive side of PC2. Here, such a separation is affected by the PC2 loading maxima at 1613 (tyrosine, isoleucine),[31,38] 1466 cm^{-1} (alanine, glutamic acid, lysine, proline, serine, and valine), and 1177 cm^{-1} (histidine) cm^{-1} attributed to various amino acids.[31] This separation may indicate various conformation of aggregates studied after 24 and 72 h of tau protein incubation. The change of structural properties, and/or secondary structure content results in different spatial arrangements of amino acid residues. The effect of structural rearrangements is specifically prominent in TERS. The resulting TER bands in collected spectra are dependent on the selection rules, which are associated with a mutual orientation of TERS probe *vs.* the polarization vector of the electric field of the incident irradiation, and the orientation of the studied molecules.

The separation along PC3 (19% of the total variance) is less evident than along PC1 and PC2. However, a major part of the spectra acquired from protofibrils after 24 h of tau incubation is located in the positive space of PC3. The positions of the PC3 loading extrema, which influenced the data separation, are characteristic of the secondary structure of proteins or specific amino acids. Specifically, the maximum at 1573 cm^{-1} is attributed to indole ring vibration in tryptophan (Trp),[41] and unordered regions of proteins or β-sheet vibrations.[20,33] The position of the 1479 cm^{-1} maximum correlates with the spectral position of CH, CH_2, CH_3, and C–N vibrations in histidine or arginine.[20,35,36] The maximum at 1171 cm^{-1} corresponds to the N–H vibration of histidine or arginine.[31,35] A well-pronounced minimum at 1532 cm^{-1} is characteristic of anti-parallel β-sheets.[20] The peak at 1434 cm^{-1} corresponds to the spectral position of CH_2, CH_3 deformational vibrations,[20,36] and histidine, or lysine.[31] The minimum at 1021 cm^{-1} is characteristic of alanine.[31]

We also performed the HCA for all acquired data. The results are presented in Fig. 4. In the HCA, based on the dendrogram, the analyzed spectra are clustered and the mean spectra for each cluster are calculated. This approach allows us to effectively compress the number of variables and inspect the differences in the characteristic spectral bands. The HCA clearly discriminated the input data into two groups: a cluster containing 85.7% of spectra acquired from protofibrils after 24 h of incubation (COMP 1), and a cluster composed in 100% of spectra collected from fibrils after 72 h of incubation (COMP 2). The mean spectra of each cluster are presented in Fig. 4B. The overall conclusion from this analysis is consistent with the PCA results. The mean spectra are differentiated mainly in the spectral region characteristic of peptide/protein backbone, specifically amide I, amide II, and amide III, which suggests alterations in the secondary structure of the studied types of tau aggregates. First, in the mean spectrum of COMP1 composed mainly of spectra acquired from protofibrils formed after 24 h of tau aggregation, the amide I bands are not well resolved. However, two clear maxima are outlined at 1576 cm^{-1} and 1525 cm^{-1}, indicating the presence of β-sheet/random coil structures and anti-parallel β-sheets, respectively.[20,33] In this spectral region, the mean spectrum attributed to young fibrils (COMP2) displays a relatively higher intensity around 1576 cm^{-1}, and the peak typical of anti-parallel β-sheets is not pronounced. The overall shapes of the amide I and amide II bands are different for COMP2. Here, the relatively intense amide I band at 1620 cm^{-1} indicating the abundance of parallel β-sheets is well pronounced. In the amide II range, the band at 1545 cm^{-1} can be distinguished suggesting the α-helix secondary structure.[33] The difference in the intensity is significant for the band at 1388 cm^{-1}. This spectral position is attributed to the C_α–H/N–H bending typical of β-sheets.[20,37] The increase in the intensity in this spectral region suggests the increase in the β-sheet secondary structure content in young fibrils. The intensity of the mean spectrum of COMP2 is also higher in the amide III region, with two well pronounced maxima at 1315 cm^{-1} and 1262 cm^{-1} assigned to CH_2 deformation vibration, and unordered regions of proteins, respectively.[22,36] The amide III band attributed to β-sheets is at *ca.* 1230 cm^{-1} in the spectrum of COMP1, suggesting the presence of anti-parallel β-sheets in the structure of protofibrils, whereas in the mean spectrum of young fibrils the position of this band shifts to 1221 cm^{-1} typical of parallel β-sheets.[22] Dissimilarity in the band position and intensity is also visible in the spectral region characteristic of specific vibrations in amino acids. Specifically, in the spectral range of 1200–1100 cm^{-1}, the mean spectrum of COMP1 (protofibrils, 24 h of tau aggregation) displays a maximum at 1175 cm^{-1} (the N–H vibration of histidine or arginine[31,35] and/or the C–H stretching of methionine[31]). This maximum is located at 1185 cm^{-1} in the mean spectrum of COMP2 (young fibrils formed after 72 h of tau incubation). This band at 1185 cm^{-1} is attributed to the C–H bending/C–O stretching vibrations of phenylalanine.[31] In both mean spectra of selected components, the band at *ca.* 1003 cm^{-1} (phenylalanine) is prominent; however, the intensity in this position is relatively higher for the mean spectrum of young fibrils. The relatively high intensity of the band at 1003 cm^{-1} together with the band at 1185 cm^{-1} in the mean spectrum of young fibrils indicate that the vibrations of functional groups in phenylalanine are oriented perpendicular to the polarization vector of the electric field of the incident irradiation, which results in the manifestation of these vibrations in the TER spectrum. All the described differences in the mean spectra of components selected in HCA suggest different spatial arrangements of the secondary structure, and thus, amino acids in the structure of tau protein protofibrils and young fibrils.

In order to uncover the meaningful features from the collected map, the Non-negative Matrix Factorization (NMF) algorithm was used. This method allows transformation of the high-dimensional data into two matrices. The most informative in this approach is matrix H, which corresponds to the chemical compounds composing the spectra and allows production of the false-color maps of its distribution. The results of the NMF analysis for the representative map are presented in Fig. 5. The NMF component of the TER spectrum displays bands characteristic of fibrillar species including amide I bands at 1649 cm^{-1} (α-helix/unstructured coils),[33] 1628 cm^{-1}

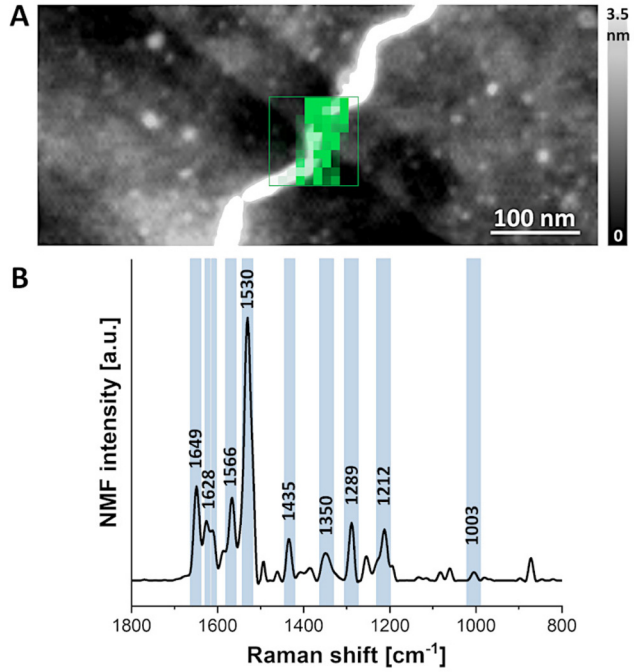

Fig. 5 TERS mapping of tau fibril: (A) AFM image of tau fibril with superimposed TERS map (green pixels) subjected to NMF analysis. The intensity of pixels corresponds to the contribution of the specific NMF component in the TER spectrum in a particular pixel. (B) The plot of the corresponding NMF component.

(parallel β-sheets),[21] and 1612 cm^{-1} (tyrosine, isoleucine),[31,38] amide II bands at 1566 cm^{-1} (random coils, fibril core β-sheets)[20,33] and 1530 (anti-parallel β-sheets),[20] and amide III bands at 1289 cm^{-1} (α-helix)[41] and 1212 cm^{-1} attributed to the parallel β-sheet secondary structure.[20,22] Moreover, well-resolved bands at 1435 cm^{-1} (CH, CH_2, CH_3 deformation),[35–37] 1350 cm^{-1} (CH_2 deformation),[35,36] and 1003 cm^{-1} (ring breathing mode of phenylalanine)[20,22,32] are distinctive for the structure of proteins.

In summary, we showed the nanoscale Raman spectra from individual tau aggregates at the growth phase, specifically protofibrils and young fibrils. The multivariate data analysis enabled the extraction of spectral differences for TERS data acquired from the studied types of tau aggregates. We confirmed that the spectral patterns of protofibrils were dominated by vibrations of antiparallel β-sheets, while the TER spectra of young fibrils were rich in bands characteristic of parallel β-sheets. The knowledge on the structural rearrangements of tau in the course of the aggregation process contributes to revealing the mechanisms of the tau aggregation and thus, designing effective therapeutic approaches against AD at early stages of the disease.

It is worth noting that our findings refer to the fibril growth conditions described here. Abnormal aggregation of amyloids including tau is a very complex process, which can be affected by a plethora of intrinsic and extrinsic factors such as a protein sequence and concentration, buffer composition, temperature, pH and also the influence of the heparin sodium characteristics (molar mass, exact elemental composition, *etc.*). Therefore, the secondary structure of the aggregates could change upon different conditions.

Author contributions

K.S.: conceptualization; K.S.: led the original draft writing; K. S., E.L., and K.S-N: manuscript editing; K.S.: funding acquisition, K.S., S.S., and E.L.: investigation; K.S., S.S., and J.B.: visualization, K.S., E.L., S.S., K.S-N., and J.B.: data analysis; K. S-N.: multivariate data analysis; K.S. and E.L.: project administration. All authors contributed to scientific discussions related to data analysis and interpretation.

Conflicts of interest

There are no conflicts to declare.

Acknowledgements

Authors would like to acknowledge Prof. Marek Szymoński for being their mentor, and for the support, advice and every discussion and conversation. This research was funded wholely by the National Science Centre, Poland, under the SONATA 17 project [Reg. No. UMO-2021/43/D/ST4/02655].

References

1 B. Winblad, P. Amouyel, S. Andrieu, C. Ballard, C. Brayne, H. Brodaty, A. Cedazo-Minguez, B. Dubois, D. Edvardsson, H. Feldman, L. Fratiglioni, G. B. Frisoni, S. Gauthier, J. Georges, C. Graff, K. Iqbal, F. Jessen, G. Johansson, L. Jönsson, M. Kivipelto, M. Knapp, F. Mangialasche, R. Melis, A. Nordberg, M. O. Rikkert, C. Qiu, T. P. Sakmar, P. Scheltens, L. S. Schneider, R. Sperling, L. O. Tjernberg, G. Waldemar, A. Wimo and H. Zetterberg, *Lancet Neurol.*, 2016, **15**, 455–532.
2 L. Mucke, *Nature*, 2009, **461**, 895–897.
3 E. E. Congdon and E. M. Sigurdsson, *Nat. Rev. Neurol.*, 2018, **14**, 399–415.
4 G. Livingston, J. Huntley, A. Sommerlad, D. Ames, C. Ballard, S. Banerjee, C. Brayne, A. Burns, J. Cohen-Mansfield, C. Cooper, S. G. Costafreda, A. Dias, N. Fox, L. N. Gitlin, R. Howard, H. C. Kales, M. Kivimäki, E. B. Larson, A. Ogunniyi, V. Orgeta, K. Ritchie, K. Rockwood, E. L. Sampson, Q. Samus, L. S. Schneider, G. Selbæk, L. Teri and N. Mukadam, *Lancet*, 2020, **396**, 413–446.
5 **https://www.alz.co.uk/research/statistics**, 2016, 1.
6 L. M. Ittner and J. Götz, *Nat. Rev. Neurosci.*, 2011, **12**, 67–72.

7 M. A. Busche, S. Wegmann, S. Dujardin, C. Commins, J. Schiantarelli, N. Klickstein, T. V. Kamath, G. A. Carlson, I. Nelken and B. T. Hyman, *Nat. Neurosci.*, 2019, **22**, 57–64.
8 K. A. Vossel, K. Zhang, J. Brodbeck, A. C. Daub, P. Sharma, S. Finkbeiner, B. Cui and L. Mucke, *Science*, 2010, **330**, 198.
9 C. A. Ross and M. A. Poirier, *Nat. Rev. Mol. Cell Biol.*, 2005, **6**, 891–898.
10 J. Hardy and D. J. Selkoe, *Science*, 2002, **297**, 353–356.
11 Z. He, J. L. Guo, J. D. McBride, S. Narasimhan, H. Kim, L. Changolkar, B. Zhang, R. J. Gathagan, C. Yue, C. Dengler, A. Stieber, M. Nitla, D. A. Coulter, T. Abel, K. R. Brunden, J. Q. Trojanowski and V. M. Y. Lee, *Nat. Med.*, 2018, **24**, 29–38.
12 H. I. L. Jacobs, T. Hedden, A. P. Schultz, J. Sepulcre, R. D. Perea, R. E. Amariglio, K. V. Papp, D. M. Rentz, R. A. Sperling and K. A. Johnson, *Nat. Neurosci.*, 2018, **21**, 424–431.
13 F. Panza, M. Lozupone, G. Logroscino and B. P. Imbimbo, *Nat. Rev. Neurol.*, 2019, **15**, 73–88.
14 K. Iqbal, F. Liu and C. X. Gong, *Nat. Rev. Neurol.*, 2016, **12**, 15–27.
15 C. M. Wischik, C. R. Harrington and J. M. D. Storey, *Biochem. Pharmacol.*, 2014, **88**, 529–539.
16 S. S. Shafiei, M. J. Guerrero-Muñoz and D. L. Castillo-Carranza, *Front. Aging Neurosci.*, 2017, **9**, 83.
17 M. D. C. Cárdenas-Aguayo, L. Gómez-Virgilio, S. DeRosa and M. A. Meraz-Ríos, *ACS Chem. Neurosci.*, 2014, **5**, 1178–1191.
18 Z. Zhang, M. Song, X. Liu, S. S. Kang, I. S. Kwon, D. M. Duong, N. T. Seyfried, W. T. Hu, Z. Liu, J. Z. Wang, L. Cheng, Y. E. Sun, S. P. Yu, A. I. Levey and K. Ye, *Nat. Med.*, 2014, **20**, 1254–1262.
19 Z. He, J. D. McBride, H. Xu, L. Changolkar, S.-J. Kim, B. Zhang, S. Narasimhan, G. S. Gibbons, J. L. Guo, M. Kozak, G. D. Schellenberg, J. Q. Trojanowski and V. M. Y. Lee, *Nat. Commun.*, 2020, **11**, 1–18.
20 E. Lipiec, J. Kaderli, J. Kobierski, R. Riek, K. Skirlińska-Nosek, K. Sofińska, M. Szymoński and R. Zenobi, *Angew. Chem.*, 2021, **133**, 4595–4600.
21 E. Lipiec, D. Perez-Guaita, J. Kaderli, B. Wood and R. Zenobi, *Angew. Chem.*, 2018, **130**, 8655–8660.
22 S. Bonhommeau, D. Talaga, J. Hunel, C. Cullin and S. Lecomte, *Angew. Chem., Int. Ed.*, 2017, **56**, 1771–1774.
23 M. Paulite, C. Blum, T. Schmid, L. Opilik, K. Eyer, G. C. Walker and R. Zenobi, *ACS Nano*, 2013, **7**, 911–920.
24 D. Kurouski, T. Deckert-Gaudig, V. Deckert and I. K. Lednev, *J. Am. Chem. Soc.*, 2012, **134**, 13323–13329.
25 F. S. Ruggeri, G. Longo, S. Faggiano, E. Lipiec, A. Pastore and G. Dietler, *Nat. Commun.*, 2015, **6**, 7831.
26 F. S. Ruggeri, J. Habchi, S. Chia, R. I. Horne, M. Vendruscolo and T. P. J. Knowles, *Nat. Commun.*, 2021, **12**, 1–9.
27 F. S. Ruggeri, B. Mannini, R. Schmid, M. Vendruscolo and T. P. J. Knowles, *Nat. Commun.*, 2020, **11**, 2945.
28 D. Kurouski, A. Dazzi, R. Zenobi and A. Centrone, *Chem. Soc. Rev.*, 2020, **49**, 3315–3347.
29 J. Szczerbiński, J. B. Metternich, G. Goubert and R. Zenobi, *Small*, 2020, **16**, 1905197.
30 T. Deckert-Gaudig, D. Kurouski, M. A. B. Hedegaard, P. Singh, I. K. Lednev and V. Deckert, *Sci. Rep.*, 2016, **6**, 24512–24520.
31 G. Zhu, X. Zhu, Q. Fan and X. Wan, *Spectrochim. Acta, Part A*, 2011, **78**, 1187–1195.
32 T. Deckert-Gaudig, E. Kämmer and V. Deckert, *J. Biophotonics*, 2012, **5**, 215–219.
33 V. A. Shashilov, V. Sikirzhytski, L. A. Popova and I. K. Lednev, *Methods*, 2010, **52**, 23–37.
34 Z. Chi, X. G. Chen, J. S. W. Holtz and S. A. Asher, *Biochemistry*, 1998, **37**, 2854–2864.
35 T. Deckert-Gaudig, D. Kurouski, M. A. B. Hedegaard, P. Singh, I. K. Lednev and V. Deckert, *Sci. Rep.*, 2016, **6**, 1–9.
36 N. C. Maiti, M. M. Apetri, M. G. Zagorski, P. R. Carey and V. E. Anderson, *J. Am. Chem. Soc.*, 2004, **126**, 2399–2408.
37 D. Kurouski, R. P. Van Duyne and I. K. Lednev, *Analyst*, 2015, **140**, 4967–4980.
38 B. Hernández, Y. M. Coïc, F. Pflüger, S. G. Kruglik and M. Ghomi, *J. Raman Spectrosc.*, 2016, **47**, 210–220.
39 F. Pflüger, B. Hernández and M. Ghomi, *J. Phys. Chem. B*, 2010, **114**, 9072–9083.
40 M. F. Rosario-Alomar, T. Quiñones-Ruiz, D. Kurouski, V. Sereda, E. B. Ferreira, L. De Jesús-Kim, S. Hernández-Rivera, D. V. Zagorevski, J. López-Garriga and I. K. Lednev, *J. Phys. Chem. B*, 2015, **119**, 1265–1274.
41 A. Rygula, K. Majzner, K. M. Marzec, A. Kaczor, M. Pilarczyk and M. Baranska, *J. Raman Spectrosc.*, 2013, **44**, 1061–1076.